

Chapter 2

Satellite Water Colour Observations in African Seas

Jim Gower and Stephanie King

Abstract Satellite water colour image data can now be used to show the spatial patterns of coastal and ocean water properties, especially surface chlorophyll concentration, on scales covering from kilometers to the entire globe. The repeated coverage shows weekly, seasonal and longer term variability, and provides a unique resource for regions where in-situ data sources are scarce, as is the case for most waters round the continent of Africa. Easy access to extensive data sets of satellite-measured chlorophyll, characterized through the average absorption and scattering properties of phytoplankton, and through natural fluorescence, are now available from Goddard Interactive Online Visualization ANd aNalysis Infrastructure (GIOVANNI), developed by the US National Aeronautics and Space Administration (NASA), and other data systems. In addition, data such as the MCI index from MEDium Resolution Imaging Spectrometer (MERIS), available by the European Space Agency (ESA), derived using spectral bands near 700 nm in the near-infrared part of the spectrum, provide further information on blooms and aquatic vegetation. We present here results of satellite observations of various African seas, showing some of the variety of observations and time series results possible.

2.1 Satellite Ocean Colour Data

“Satellite water colour data” refers to the relatively low (typically 1 km) spatial resolution optical image data of oceans and coastal waters provided by specialized satellite imagers. Data are collected in carefully chosen spectral bands, typically 10–20 nm wide. Land imaging usually requires higher spatial resolution (to 30 m or less) and often uses broad spectral bands (100 nm) or even the full available optical window (panchromatic images). Important requirements for water imaging are frequent repetition, with the satellites providing near-daily coverage, though frequently interrupted by cloud, and precise short and long-term calibration.

The US ocean colour satellite sensors Coastal Zone Color Scanner (CZCS), Sea-viewing Wide Field of view Scanner (SeaWiFS), MODerate Resolution Imaging

J. Gower (✉) · S. King

Institute of Ocean Sciences, Fisheries and Oceans Canada, Sidney, BC V8L 4B2, Canada
e-mail: Jim.Gower@dfo-mpo.gc.ca

Spectroradiometer (MODIS) and Visible/Infrared Imager Radiometer Suite (VIIRS), and the European sensor MEdium Resolution Imaging Spectrometer (MERIS) provide global data on ocean and coastal near-surface phytoplankton concentration at spatial resolutions down to 1 km (300 m for MERIS) over image swaths 2,000 km across (3,000 km for VIIRS, 1,100 km for MERIS). These have been joined for short periods by sensors from several other countries. The Indian Ocean Colour Monitor (OCM) has provided some data since launch in 1999 on the Indian Oceansat-1 satellite, and a follow-on instrument (OCM 2) was launched in 2009 on Oceansat-2.

Optical data from these satellites are used primarily to deduce chlorophyll concentrations in near-surface waters. Chlorophyll is a standard indicator of phytoplankton concentration, which in turn represents the primary-producing biomass at the base of the marine food chain. Images can be used to examine spatial patterns of high-chlorophyll in upwelling zones and blooms, or conversely “ocean deserts” in centres of mid-ocean gyres, where chlorophyll concentrations are low. The images show seasonal patterns, for example those due to coastal upwelling driven by seasonal winds, or the spring bloom in extra-tropical waters. On longer time scales, they may also show how bloom frequency or extent are affected by global warming, changing nutrient input, or the spread of new species in ship’s ballast water. In some cases blooms are triggered by mixing after intense storms, or by nutrient input from rivers, volcanic eruptions or artificial fertilization. Timing and intensity of patterns of measured chlorophyll can then be related to fish catch and properties of marine ecosystems.

Chlorophyll concentrations are deduced from the satellite optical data by measuring the combined effects of increased scattering near 550 nm (green light) and increased absorption near 450 nm (blue light). Increased phytoplankton concentration causes more scattering from cell walls and other structural parts of the organisms, which increases the amount of green light back-scattered from the ocean. At the same time, more absorption due to higher concentrations of chlorophyll-*a* and auxiliary pigments responsible for energy gathering for photosynthesis reduces the amount of blue light. This “blue to green” ratio is used to deduce chlorophyll concentrations from observed spectral radiances. The relation is well-determined in “Case 1” waters, defined as those whose varying optical properties are determined by phytoplankton and not by the presence of other constituents such as suspended sediments or dissolved organic material, or again by bottom reflection in shallow water.

In addition to deducing chlorophyll content, optical sensors can measure water reflectance, for example in green light near 550 nm, and use this to deduce the total amount of scattering material in the water. If this is found to be higher than expected for the measured amount of phytoplankton, then the water can be flagged as “Case 2” (essentially anything other than Case 1) and the higher scattering can be related to sediment from rivers, or resuspension from the bottom in shallow water. In some cases, high back-scatter can be due to blooms of species such as *Coccolithophores*, which are considered Case 2 because of the extreme brightness of their blooms. Concentration of Coloured Dissolved Organic Material (CDOM) can also be deduced from measured radiances at the shortest wavelengths, typically 412 nm. Waters with significant concentrations of CDOM are also classed as Case 2.

In order to measure the actual reflectance of water, the water-leaving radiances have to be computed from those measured at the satellite. This involves computing the

radiance added by scattering in the atmosphere and the radiance lost due to absorption, that is, atmospheric correction has to be applied. This is conventionally referred to as deriving “Level 2” data (atmospherically corrected radiances, reflectances and derived products), from “Level 1” (radiances measured by the satellite). Level 1 to Level 2 conversion also tries to correct for sun-glint, sky reflection and light transmission at the water surface. “Level 0” refers to the raw data packets transmitted from the satellite, whose redundancies and encodings make them less useful for applications. “Level 3” refers to image composites covering particular time periods (often 8-day, or monthly), or larger, often global, areas. “Level 4” is sometimes used to refer to products derived from satellite data, but with addition of information from other sources. A subdivision of Level 1 to Levels 1A and 1B is used to denote pixel location (latitude and longitude) information added in 1B.

The major component of atmospheric correction is due to Rayleigh scattering by atmospheric gases, which can be computed knowing the viewing geometry of the scene, the sun and the sensor. Precise calculation requires exact calibration of the sensor, including detailed knowledge of its polarization sensitivity, and also accurate atmospheric pressure at the ocean surface. The much more variable component due to aerosol scattering requires added measurements, which over water can be provided by the same sensor using wavelengths longer than 700 nm, where signal from the water is usually negligible. These measured radiances therefore show the strength and spectral properties (Angstrom coefficient, if a simple power-law) of the aerosol component, which can then be extrapolated to shorter wavelengths at which water-leaving radiances are significant. Measurements at the shortest wavelengths are the most problematic, causing problems for estimates of CDOM.

2.2 Chlorophyll Fluorescence Measurements from Satellites

We also present here results from measurements of chlorophyll fluorescence which can be made by more recent sensors such as MODIS and MERIS (but not VIIRS) using bands near 683 nm (Gower and Borstad 1990; Abbott and Letelier 1999; Gower and King 2007a). Measurements are made in the wavelength range where fluorescence is emitted (675–695 nm), and also at nearby wavelengths where fluorescence is absent or much reduced, to give background reference radiances. Oxygen absorption at wavelengths longer than 687 nm needs to be avoided, so MODIS measures fluorescence at 673 nm, and MERIS at 681 nm, shorter wavelengths than otherwise preferred. In both cases, fluorescence is measured as Fluorescence Line Height (FLH), computed as radiance at a central wavelength, above a reference radiance linearly interpolated from two adjacent bands, one at a shorter wavelength and one at a longer. For MODIS, measurements are made at 665, 673 and 748 nm and for MERIS at 665, 681 and 709 nm. For large-area studies, FLH is computed from Level 2 data, but the atmospheric correction for FLH is relatively small, and FLH values are often computed from Level 1 radiances. This has the advantage of avoiding problems with atmospheric correction, which are usually more severe in coastal areas, but requires a method for rejecting data affected by cloud or strong sun glint. For MERIS, a typical

relation (Gower and King 2007a) is:

$$\begin{aligned} \text{if } L_{865} < 15 \text{ mW m}^{-2} \text{ sr}^{-1} \text{ nm}^{-1}, \\ \text{then } \text{FLH} = L_{681} - L_{665} - 0.364 (L_{709} - L_{665}) \end{aligned} \quad (2.1)$$

where L_{865} represents Level 1 radiances (as measured at the satellite) at a wavelength of 865 nm, and similarly for other wavelengths, and the factor 0.364 represents the wavelength ratio $(681-665)/(709-665)$. For MODIS, bands are different, as noted above, and the factor becomes 0.096.

It is often assumed that the measured fluorescence signal will increase with sun elevation, and this is compensated by normalizing FLH to what would be observed had the sun been at zenith (NFLH), that is $\text{NFLH} = \text{FLH}/\cos(Z)$, where Z is the zenith angle of the sun at the time of observation. In fact, we show below that normalization is not appropriate.

We have suggested that fluorescence is proportional to chlorophyll concentration at low concentrations, but saturates due to absorption of both stimulated and emitted radiation at higher concentrations (Gower et al. 2004; Gower and King 2007a). For FLH computed from Level 1 data, we propose

$$\text{FLH} = (0.18C/(1 + 0.2C)) - 0.24 \quad (2.2)$$

as a good average relation between chlorophyll (in mg m^{-3}) and fluorescence in radiance units ($\text{W m}^{-2} \text{ nm}^{-1} \text{ ster}^{-1}$). The offset, here given as -0.24 , is variable, depending on viewing and atmospheric conditions. The factor 0.2 is the ratio of absorption of fluorescence by 1 mg m^{-3} of chlorophyll, to the absorption of fluorescence by water. The term appears in equation (2.2) by analogy with the relation $R = k \times b/a$ for water reflectance (Morel and Prieur 1977). This factor expresses the fact that FLH increases less rapidly with C , as C increases. At a value of $C = 20 \text{ mg m}^{-3}$ the rate is reduced by a factor 5 from the value at low C . At higher values, the combination of water and chlorophyll absorption results in a radiance peak near 700 nm for $C = 30 \text{ mg m}^{-3}$, and near 710 nm for $C = 300 \text{ mg m}^{-3}$, which prevents observation of fluorescence.

2.3 Detection of Blooms and Vegetation Using MCI

MERIS provides the Maximum Chlorophyll Index (MCI), useful for detecting concentrated surface blooms and floating vegetation. MCI measures a radiance peak at 700–710 nm. The index is unique to MERIS, in that MODIS and VIIRS do not have a band near 709 nm. The peak indicates the presence of a high surface concentration of chlorophyll-a against a scattering background (Gitelson et al. 1992; Yacobi et al. 1995; Gower et al. 1999, 2005, 2008a, b). MCI is high in “red tide” conditions (intense, visible, surface plankton blooms), and also when aquatic vegetation is present leading to a “red edge” step increase in radiance. For some blooms, the peak dominates the spectrum, giving a radiance change due to the bloom that is over ten times greater at 709 nm than at any other wavelength. We have demonstrated use of the MCI to detect plankton blooms (Gower et al. 2005), floating *Sargassum*

(Gower et al. 2006; Gower and King 2011) and “superblooms” of Antarctic diatoms associated with platelet ice (Gower and King 2007b).

The MCI is computed as radiance at 709 nm above a linear baseline defined by radiances at 681 and 753 nm (Gower et al. 2005, 2008b). As for FLH, this is calculated only for pixels for which radiance at 865 nm is less than $15 \text{ mW m}^{-2} \text{ sr}^{-1} \text{ nm}^{-1}$ to eliminate land pixels and areas of strong sun glint, haze or cloud:

$$\begin{aligned} &\text{if } L_{865} < 15 \text{ mW m}^{-2} \text{ sr}^{-1} \text{ nm}^{-1}, \\ &\text{then } \text{MCI} = L_{709} - L_{681} - 0.389 (L_{753} - L_{681}) \end{aligned} \quad (2.3)$$

where L_{865} represents Level 1 radiances (as measured at the satellite) at a wavelength of 865 nm, and similarly for other wavelengths, and the factor 0.389 represents the wavelength ratio $(709-681)/(753-681)$.

The MCI therefore indicates an excess radiance at 709 nm above this baseline, which often indicates a water-leaving radiance spectrum with a peak at 709 nm. Models indicate that this type of spectrum is characteristic of intense surface plankton blooms in which high concentrations of phytoplankton are distributed in near-surface waters. In this case, the absorption by chlorophyll reduces radiance at wavelengths shorter than 700 nm, while absorption by water reduces radiance at wavelengths longer than 720 nm, leading to a radiance peak at the wavelength of minimum absorption, near 709 nm. Models also show that vegetation under a shallow layer of water, including coral reefs, can give rise to a spectral peak near 709 nm, also giving a positive MCI signal.

MCI can also be high due to presence of a “red-edge” in the spectrum. At this “edge,” water-leaving radiance shows a step increase near 700 nm with increasing wavelength. This type of spectrum is characteristic of land vegetation, for which the red-edge (maximum rate of increase of observed radiance with wavelength) usually occurs at a longer wavelength of about 720 nm. Over water with MERIS, we observe an apparent step increase between 681 and 709 nm. The MCI as defined in Eq. 2.1 will give a high value in this case as well as in the case of a peak. We interpret red-edge type spectra as showing presence of buoyant slicks of either phytoplankton or macroalgae such as pelagic *Sargassum*.

We make use of daily, global composites of MCI data produced by the Grid Processing on Demand (G-POD) facility of ESA (Gower et al. 2008b). These have a spatial resolution of 5 km. Each composite pixel shows the maximum MCI value computed for any RR MERIS (1.2 km) pixel assigned to that composite pixel on that day. The reduced spatial resolution results in smaller blooms being spatially distorted, but the use of the maximum values in the composite preserves the record of their occurrence.

Daily composites are combined into monthly products, also at 5 km resolution, recording the maximum MCI value measured in the month. This gives complete spatial coverage in most areas and preserves information on detected blooms and vegetation. The monthly products also show presence or absence of water, and so can be used to measure water area.

The monthly composites can also be analyzed for “total MERIS count” by computing the sum of the number of MCI values above a threshold, multiplied by the

amount by which MCI exceeds its background value (in $\text{mW m}^{-2} \text{nm}^{-1} \text{sr}^{-1}$), i.e.

$$\text{MERIS count} = \sum_{m=b+t}^{m=\infty} (m - b)n(m) \quad (2.4)$$

where $n(m)$ is the number of pixels in the area having an MCI value of m , b is the background value of MCI corresponding to open water and t is the threshold value. The MERIS count can then be used to assess annual and interannual variations in bloom intensity. Timing can also be computed in terms of a peak month:

$$\text{Peak month} = \sum_{m=1}^{m=12} m.M(m) / \sum_{m=1}^{m=12} M(m) \quad (2.5)$$

where months are represented by $m = 1-12$, the total MERIS count in each month is $M(m)$ and the peak month is expressed as a number including fractions of a month. The range of months included in the sums is usually restricted to near the time of peak values in M .

2.4 Data Availability for Regional Studies

While satellite data at Level 2 has all the required information for applications by users, the data are still segmented by the satellite's orbital patterns, large in volume and generally inconvenient to use. Global composites (Level 3 data) are more convenient, but still involve handling large volumes of data. A very convenient tool is the Goddard Interactive Online Visualization ANd aNalysis Infrastructure (GIOVANNI), developed by NASA¹ (Acker and Leptoukh, 2007). Other similar tools are available from NOAA² and the Colorado Center for Astrodynamics Research at the University of Colorado³. The equivalent tool for MERIS data is ESA's G-POD system as mentioned above, but this is not publicly available on the web.

We present here satellite water colour images and data for seas round the African continent. In Sect. 5, results are derived from GIOVANNI, showing chlorophyll data (derived through standard, green to blue ratio algorithms) and fluorescence (derived as shown in Eq. 2.1) from the MODIS version onboard the Aqua orbital platform (MODIS Aqua). These data show the seasonal patterns of surface chlorophyll, indicating coastal productivity variations in response to upwelling and other mechanisms. Comparison of chlorophyll and fluorescence data show a general correlation between these two types of data, with major differences due to an error in the present way fluorescence is derived and presented, as we discuss below. When this error is removed, the two data types show good agreement in many cases. In others, the differences suggest a problem in one or other data type. These differences need to be understood, and may lead to useful new knowledge.

¹ Available at <http://disc.sci.gsfc.nasa.gov/giovanni/overview/index.html>

² Available at <http://las.pfeg.noaa.gov/oceanWatch/oceanwatch.php>

³ Available at http://eddy.colorado.edu/ccar/modis/color_global_viewer

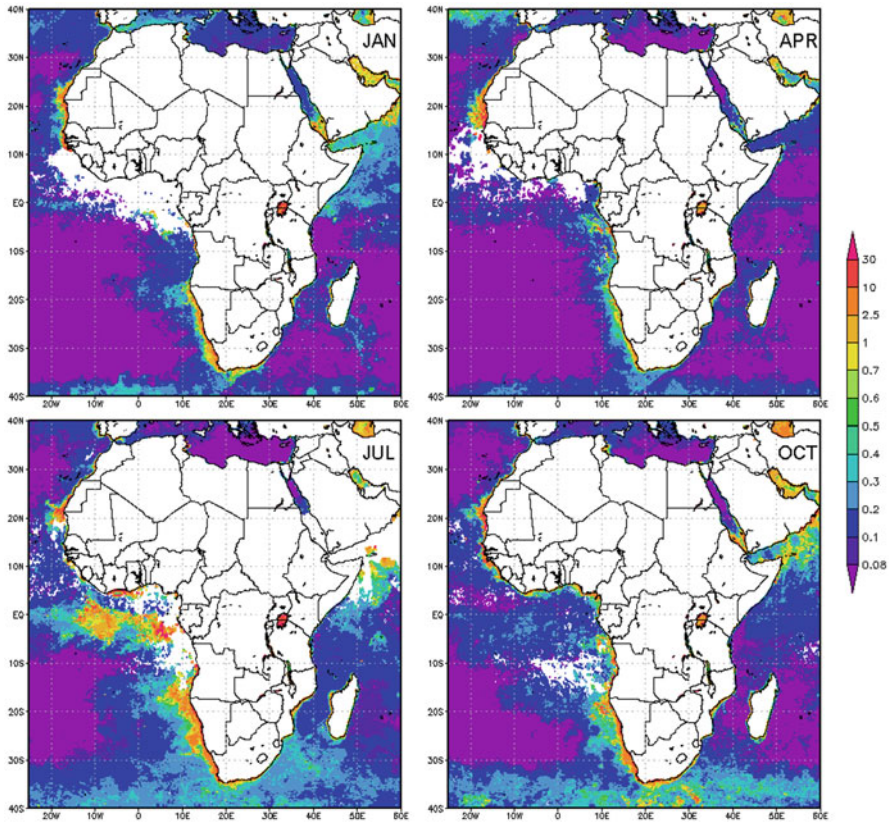


Fig. 2.1 Average surface chlorophyll concentrations round the continent of Africa in January (*top left*), April (*top right*), July (*bottom left*) and October (*bottom right*) of 2011. (MODIS Aqua data)

It has been suggested that wind-blown dust from the Sahara and other African and Asian desert areas may be a problem for remote sensing of some African waters. However, although dust contributes to marine productivity (see e.g. Singh et al. 2008), and hence affects the observed water colour, the signal from dust itself can be compensated in Level 1 to Level 2 processing (see e.g. Moulin et al. 2001). Also, dust events are always intermittent and tend to cause a smaller reduction of satellite coverage than do clouds.

2.5 African Ocean and Coastal Chlorophyll

Figure 2.1 shows the average surface chlorophyll round the continent of Africa as measured by MODIS Aqua (9-km data, downloaded from the NASA GIOVANNI data system; note the colour scale for chlorophyll-a concentration in units of mg m^{-3}

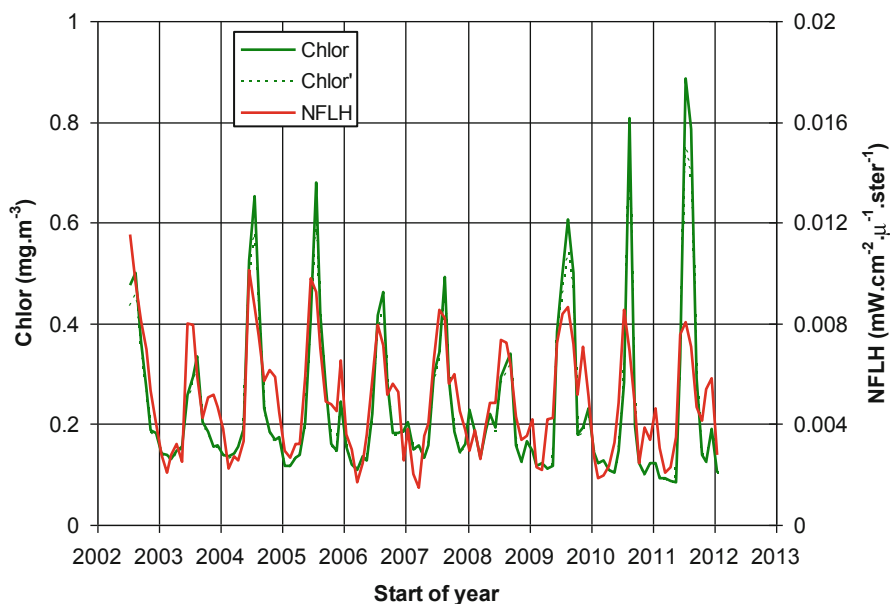


Fig. 2.2 Average surface chlorophyll concentrations (*green*) and normalized fluorescence (*red*) from MODIS Aqua data in the Gulf of Guinea, from 3°N to 3°S and 20°W to 0°

shown at right) in the months of January, April, July and October of 2011. Land is masked as white. Ocean areas which are cloudy for the entire month, such as in the Gulf of Guinea in January and in the Arabian Sea in July, are also masked to white. The bright purple areas represent the lowest surface chlorophyll, less than 0.05 mg m^{-3} (see colour scale at right). A belt of high chlorophyll covers all latitudes at 40°S at all seasons. Areas of high chlorophyll along the equator especially in July in the Gulf of Guinea in the Atlantic and to a lesser extent in the Indian Ocean, indicate the effect of equatorial upwelling. Narrow bands of high chlorophyll near shore indicate coastal upwelling in many areas, such as along the coasts of Namibia and western South Africa near 30°S, 15°E, the Horn of Africa near 10°N, 50°E and west Africa near 20°N, 15°W.

Figure 2.2 shows time series of MODIS Aqua data averaged by GIOVANNI over the area 3°N to 3°S and 20°W to 0°W along the equator in the Gulf of Guinea. Of the nine years for which MODIS Aqua so far provides data, maximum chlorophyll (green line in Fig. 2.2) is in August in 5 years, July in three and September in one, confirming the annual cycle apparent in Fig. 2.1. Fluorescence data (red line) peak slightly earlier, in July of all years except 2003 to 2005 (June) and 2009 (August). At the relative scaling of the two plots (50:1 when units are mg m^{-3} and $\text{W m}^{-2} \text{ nm}^{-1} \text{ ster}^{-1}$), the green peaks tend to be higher than the red. When comparing the green and red plots, allowance needs to be made for the expected self absorption of fluorescence as expressed in Eq. 2.2. A modified chlorophyll (i.e. Chlor': "fluorescing

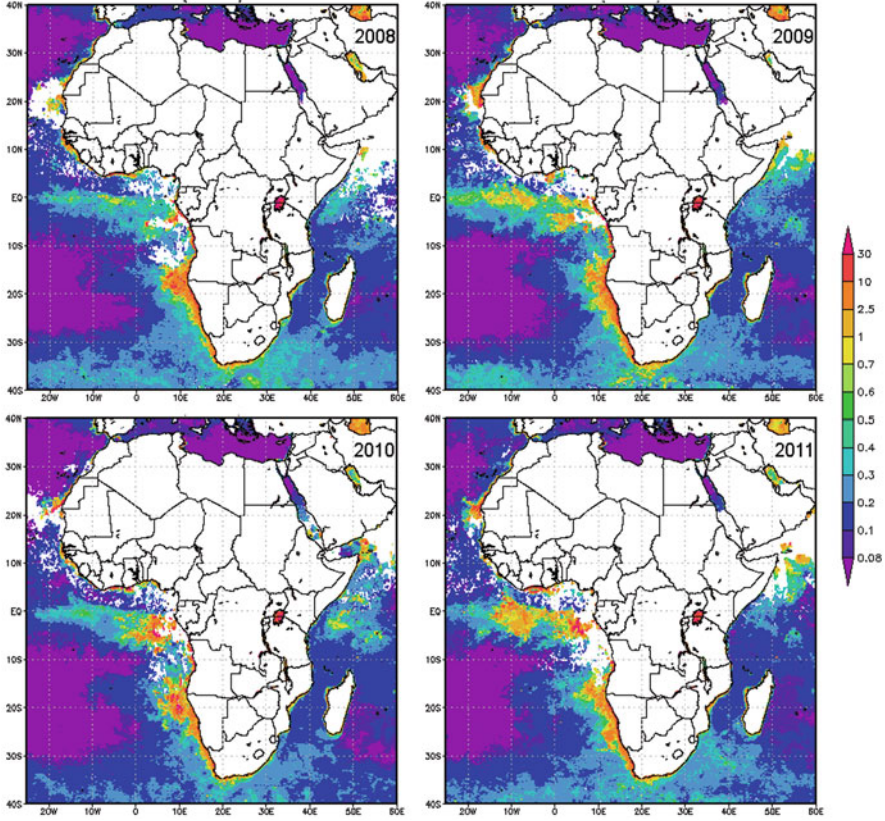


Fig. 2.3 Average surface chlorophyll concentrations round the continent of Africa in July of 2008 (top left), 2009 (top right), 2010 (bottom left) and 2011 (bottom right). (MODIS Aqua data)

chlorophyll”) is therefore also plotted (green dotted line) for which the chlorophyll value is reduced by the factor $C/(1 + 0.2 C)$, where C is the chlorophyll concentration in mg m^{-3} . In Fig. 2.2, the effect is relatively small.

A second smaller peak appears later in most years in both chlorophyll and fluorescence, but is higher in the fluorescence than in chlorophyll in all years. The relation between these two variables may indicate an average change in fluorescence yield with season, for example, the later peak may be at a time of higher nutrient stress on the phytoplankton, leading to relatively more fluorescence.

Figure 2.3 shows the July distribution in the years 2008, 2009, 2010 and 2011. The major high-chlorophyll areas are present in all years, but with significant changes in extent and concentration. Figure 2.4 shows the series of averages for the Horn of Africa, where high values are seen in Figs. 2.1 and 2.3. Figure 2.4 shows the interannual variability of chlorophyll and hence of coastal primary productivity. The high chlorophyll peaks occur each year from June to September, i.e. the cloudy season

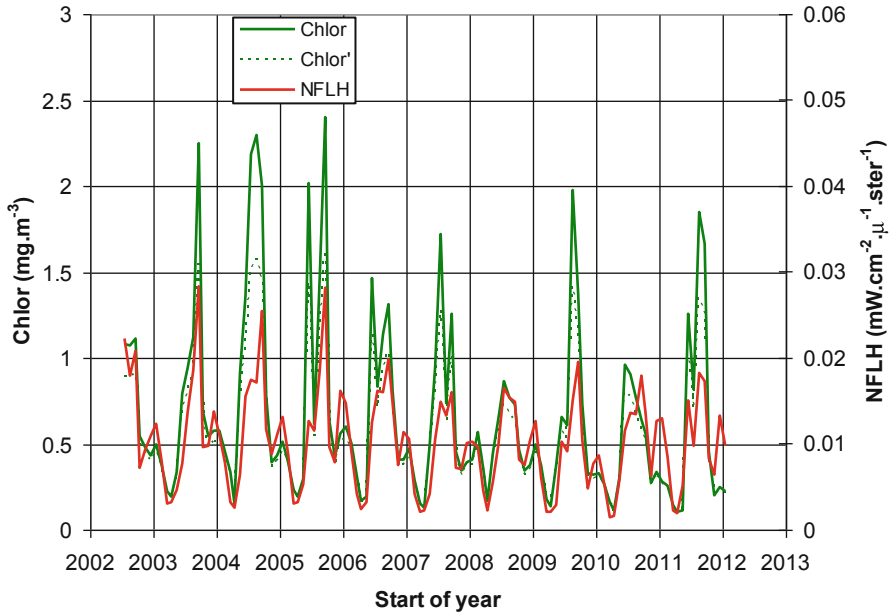


Fig. 2.4 Average surface chlorophyll concentrations (*green*) and normalized fluorescence (*red*) from MODIS Aqua data over the rectangular area off the Horn of Africa (Somalia), defined by 5–15°N and 50–55°E. Relative scaling as in Fig. 2.2

(Fig. 2.1). Variability in the peak heights, in both chlorophyll and fluorescence, will be partly due to varying amounts of cloud cover. The two time series are again very similar, apart from the higher and variable green peaks. These peaks are now significantly reduced when fluorescence absorption is included (dotted lines). Again, later peaks in the year tend to show higher values in fluorescence (red). Figure 2.5 shows results from the area off the west coasts of Angola and South West Africa, for which Figs. 2.1 and 2.3 show high chlorophyll in July and October. Clouds are much less frequent in this area, so the satellite results should give a good representation of true interannual variability. The year 2010 shows a significantly higher peak value than any other year. Peaks are in September of five years, in August of 2003, 2008 and 2010, and June and October of 2005.

The dotted green line shows a significant drop for fluorescing chlorophyll in this case, as per Eq. (2.2), but fluorescence values are still lower by about a factor 5. This may indicate conditions of ample nutrients due to coastal upwelling leading to reduced fluorescence, or it may indicate a problem with one of the two estimates of surface chlorophyll. The area includes coastal waters for which the high “blue-to-green ratio” chlorophyll estimate is not confirmed by the fluorescence data. Removing normalization (dotted and solid red lines) has only a small effect at these equatorial latitudes, as it would do in Figs. 2.2 and 2.4 (not shown).

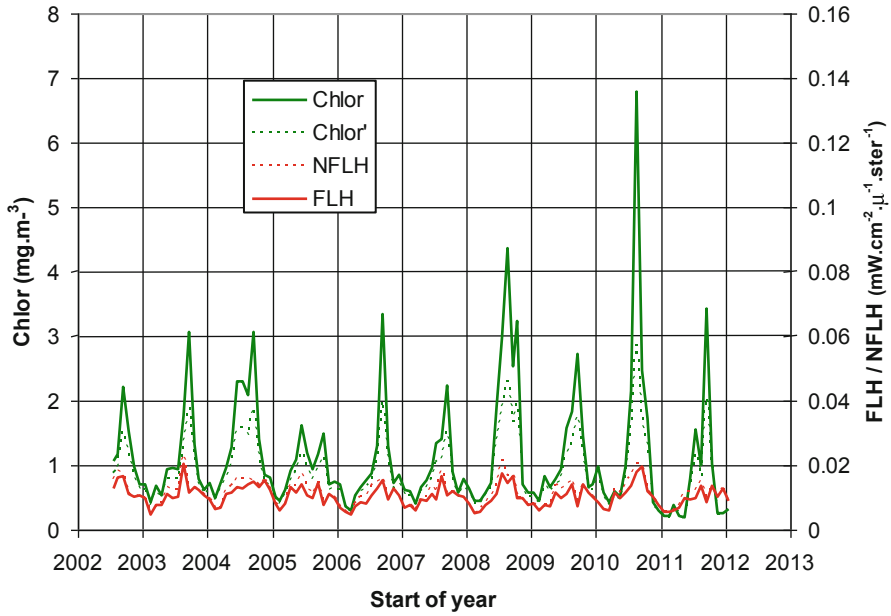


Fig. 2.5 Average surface chlorophyll concentrations (*green*) and normalized fluorescence (*red*) from MODIS Aqua data off the coasts of Angola and South West Africa, from 10 to 20°S and 5 to 15°E. Relative scaling as in Fig. 2.2

Figure 2.6 compares chlorophyll and fluorescence data averaged over 39–41°S, 10–30°E, in the area of maximum chlorophyll at the bottom of Figs. 2.1 and 2.3. The chlorophyll time series shows sporadic peaks with little clear annual cycle, but with a tendency for higher values in November to February. The normalized fluorescence time series (NFLH, dotted red) shows the reverse tendency, with a strong annual cycle, peaking near June, the season of lowest insolation. In fact, the normalization applied to fluorescence is responsible for almost the entire apparent annual cycle. With this normalization removed, the solid red line in Fig. 2.6 shows better, but still far from perfect agreement with the chlorophyll data.

Use of satellite fluorescence data has been discussed by Behrenfeld et al. (2009). It appears that fluorescence is fully stimulated by intensities of sunlight provided by all sun elevations above about 20°, which is the minimum elevation for which satellite results are computed. Behrenfeld et al. (2009) show a model with this saturation and with fluorescence quantum efficiency varying inversely with light intensity, as implied by full stimulation and as we find in these data. It is clear that FLH and not NFLH provides the better measure of chlorophyll. However, this has not yet been incorporated in NASA's satellite data processing.

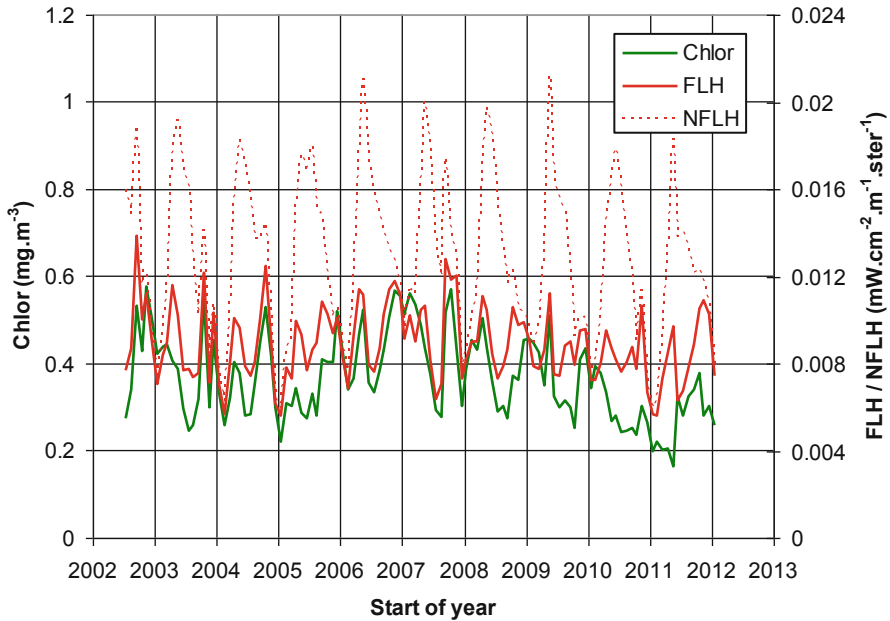


Fig. 2.6 Average surface chlorophyll concentrations (green) and fluorescence (red), plotted as normalized fluorescence (dotted red) and as-measured FLH (solid red), from MODIS Aqua data south of South Africa, from 39 to 41°S and 10 to 30°E. Relative scaling as in Fig. 2.2

2.6 Trichodesmium in the Red Sea

Figure 2.7 shows a pseudo-colour image of MCI signal in the Red Sea on 30 July 2005 near 23°N. The curved streaks are due to surface slicks of *Trichodesmium* that commonly blooms at this season. Small areas of high MCI signal near shore are due to coral reefs, whose zooanthellae also show the chlorophyll reflectance signature detected by this index.

The spectra in Figs. 2.8 and 2.9 show the “red edge” of vegetation near 700 nm with increased radiance at longer wavelengths consistent with the buoyant slicks formed by *Trichodesmium*. The spectra also show broad peaks between 500 and 620 nm which would be expected from detached trichomes in the water.

Figure 2.10 shows the monthly time series of total MCI signal for open water in the Red Sea. The monthly data show a peak near northern mid-summer in all years. The peak was large in 2005 at the time of Fig. 2.7, and even larger in 2006. On average the peaks are almost equal in June and July, but are down to 50 % of this level in August and 40 % in May. Amplitude is 15 % in April and small in other months. Peak MCI signal was reached in May in 2009 and 2010, in June in 2004, 2006, 2007 and 2011, in July in 2002, 2003 and 2005, and in August in 2008. Figure 2.11 shows the

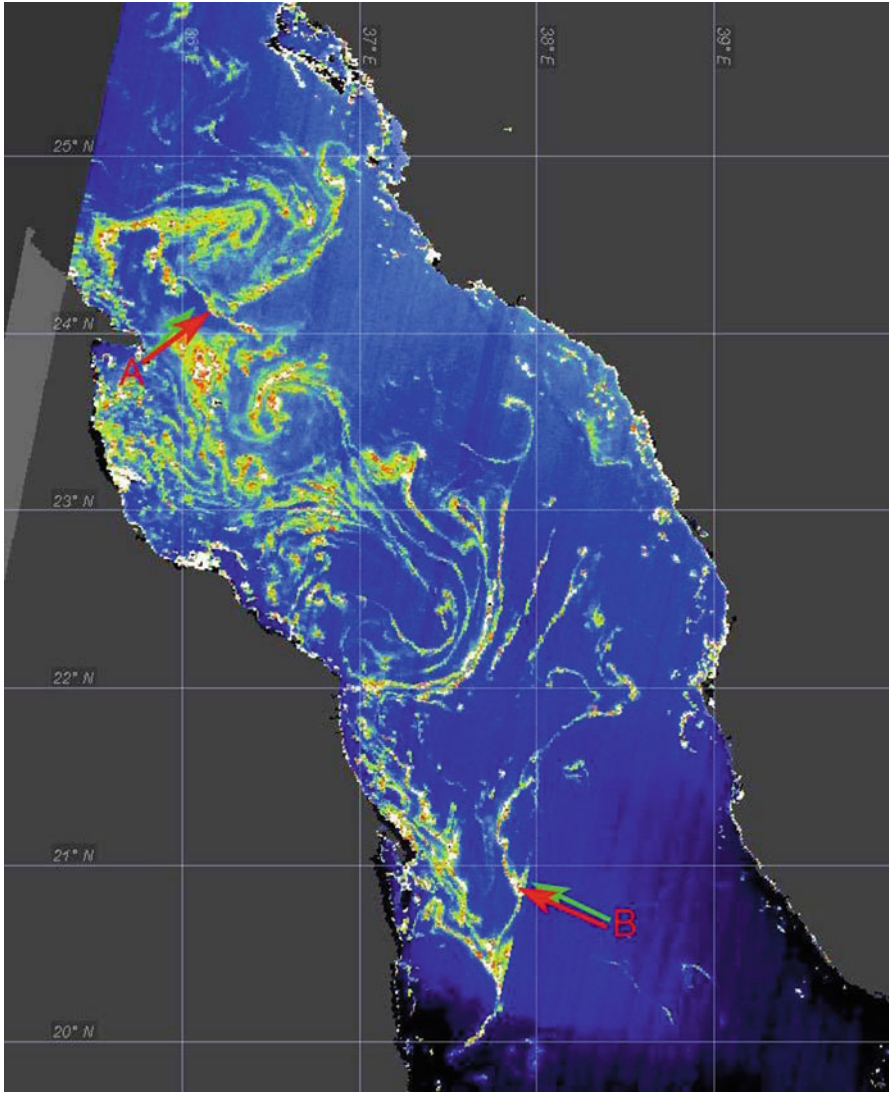


Fig. 2.7 Surface slicks of *Trichodesmium* in the Red Sea on 30 July 2005 between 20 and 25 N latitude show as areas of high MCI. This is a pseudo-colour image in which MCI radiance values are represented by a rainbow colour sequence with dark blue as the lowest signal level

average peak month for each year computed as in Eq. 2.3 using signal levels from April to August. The plot suggests a possible tendency for blooms to be happening earlier, in that the most recent three years show the three earliest computed average peak month values.

Fig. 2.8 Level 1 radiance spectra at points indicated by arrows (A) in Fig. 2.7. The red spectrum is of water containing *Trichodesmium*; the green spectrum of nearby “clear” water; the blue spectrum is the difference, showing the added radiance from the surface slick of *Trichodesmium* (right axis on expanded scale). The points indicate MERIS bands where radiances are measured

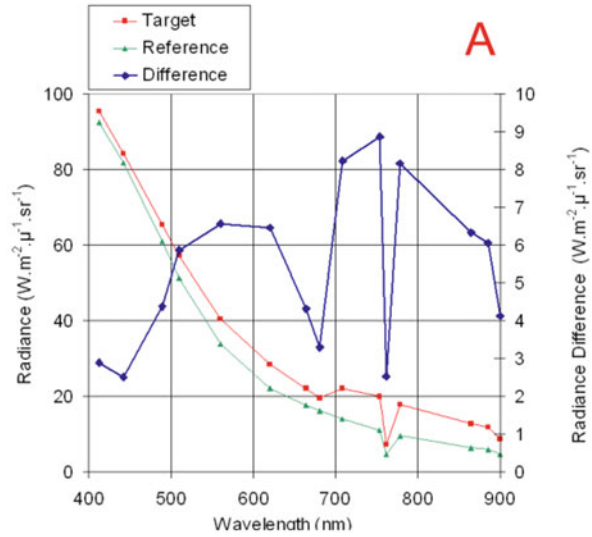
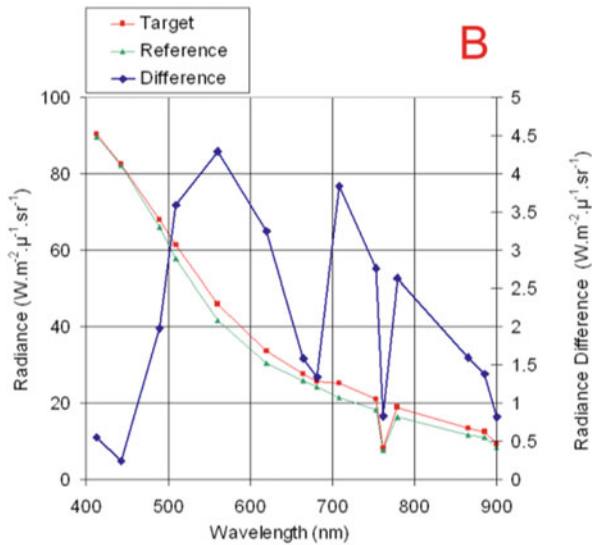


Fig. 2.9 As for Fig. 2.8, but for location B showing a similar *Trichodesmium* signature, here with relatively more detached trichomes causing a relatively larger peak at 500–620 nm



2.7 *Trichodesmium* Off Zanzibar

An intense bloom of *Trichodesmium* was reported in the channel between Zanzibar and mainland Tanzania, in the period from 3 to 15 January 2011. The monthly MERIS MCI time series for the area showed a significant MCI event in December 2010, but nothing in January 2011 (Fig. 2.12). There are extensive coral reefs in the area, but data for Fig. 2.12 were chosen to exclude these. Maximum bloom activity as shown

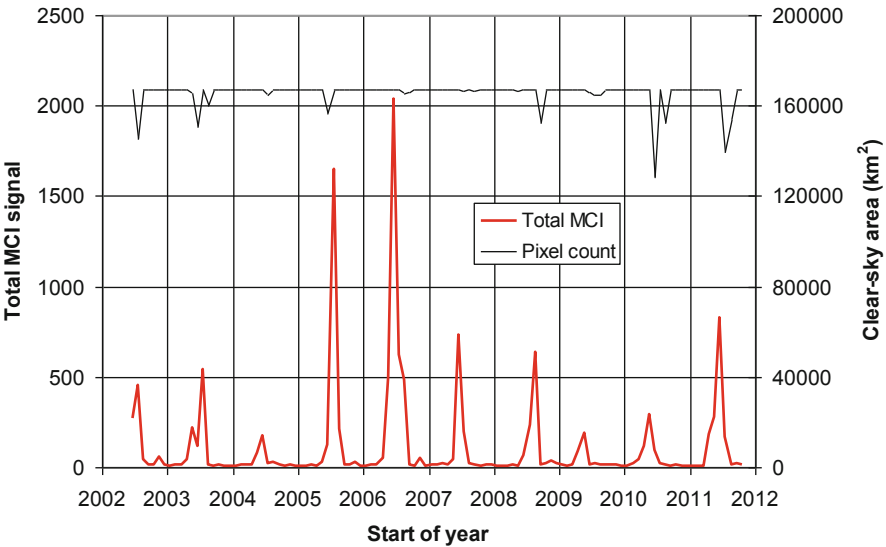


Fig. 2.10 Total MCI signal (*red*) and clear sky area (*black*) in a strip of water about 170 km wide and 1,000 km long, down the axis of the Red Sea from 27 N, diagonally across the area of Fig. 2.7, to about 17 N

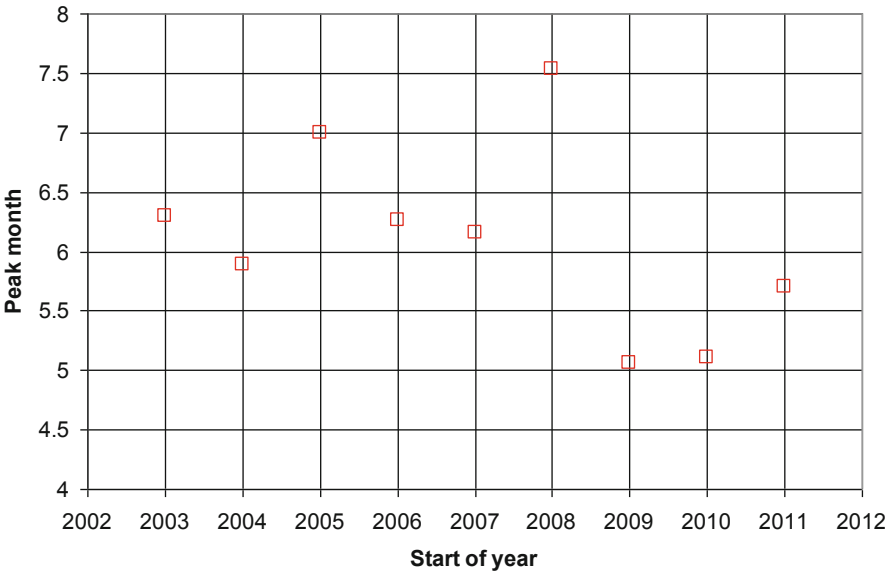


Fig. 2.11 Peak bloom month computed from the total MCI signal used in Fig. 2.10

by MCI occurs from October to January in all years since 2006, but in September 2005 and March 2003, with low signal in 2004. December 2010 stands out for the highest total MCI signal in the 10-year MERIS dataset, indicating intense, extensive

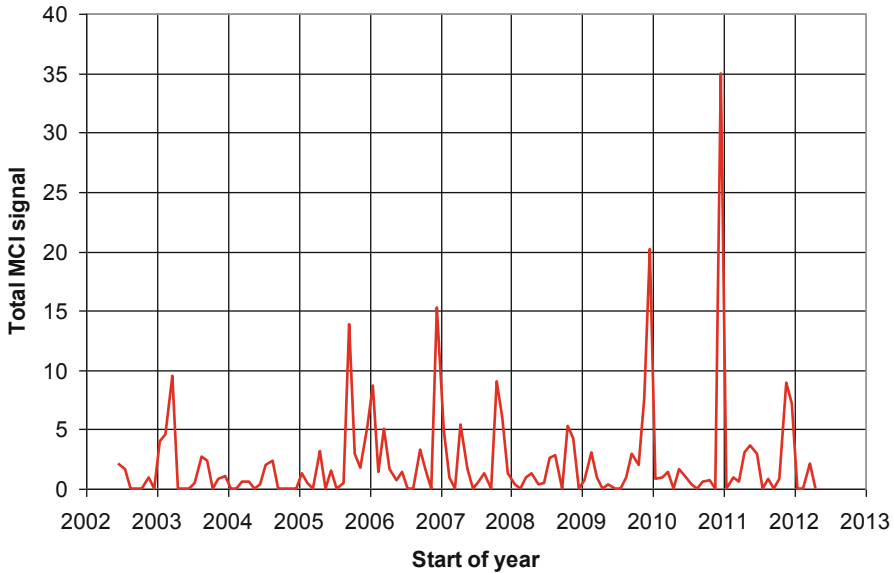


Fig. 2.12 Total MCI signal in a strip of water about 25 km wide, south of the island of Zanzibar off the coast of Tanzania, east Africa, and extending south-west about 100 km into the Indian ocean

blooms south of Zanzibar Island. Lesser events were recorded in Decembers of 2006, 2009 and 2011. The daily composite images show that the December event was imaged just on a single day, December 27. There are clear images on December 16 and 19, which show no event, and a partly cloudy image on December 30, which also shows nothing. Images of the area on January 15, 18 and 29 show small bloom activity outside the area used for Fig. 2.12.

Figure 2.13 shows MERIS data (at 1.2 km reduced resolution) of the event on December 27. Level 1 spectra are plotted from the observed radiances, with no atmospheric correction, for both a pixel with bloom (red arrow) and a nearby reference pixel with no apparent bloom indicated by MCI (green arrow). The difference spectrum (blue line, right axis) shows the bloom signature as a change in spectral radiance. MERIS shows bloom signals on both December 27 and January 15, but about ten times more strongly on December 27. The images suggest that in situ reports from Zanzibar missed the peak of the event. Sun glint, clouds and the relatively narrow MERIS swath reduce coverage to only 3–6 images of the area per month. The bloom might also have been dispersed by wind events. MERIS suggest an intense bloom period in late December with the bloom dispersed by December 30, with some residual bloom activity over the next 2 weeks.

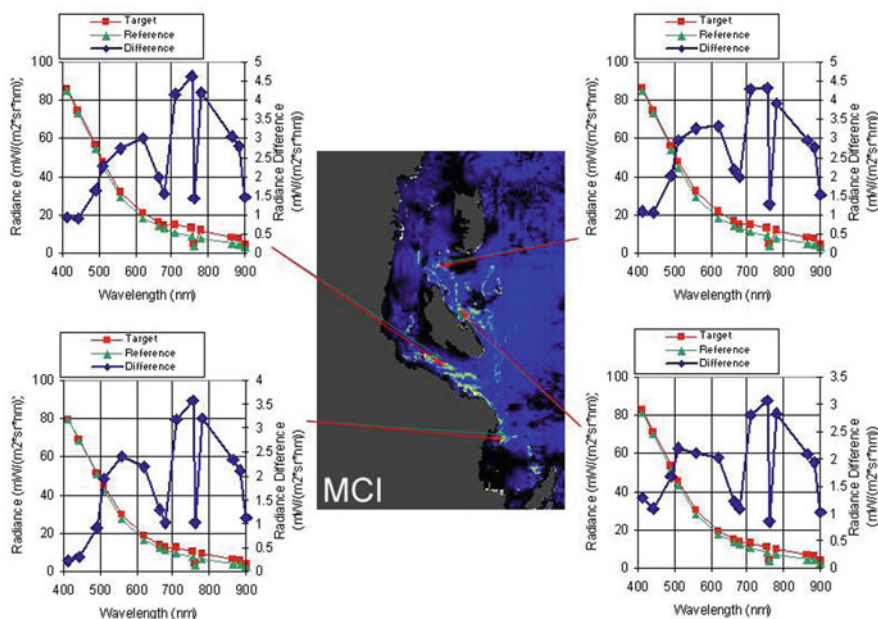


Fig. 2.13 MERIS RR level IMCI image for the Tanzania coast with the island of Zanzibar (Unguja Island, *centre*) with the similar-sized island of Pemba to the north of it. Spectra for the four areas all show the chlorophyll red edge at 700 nm, indicating a slick of floating bloom or other vegetation. Figure 2.12 shows data for the area of the *top left* spectrum, south of Zanzibar

2.8 Trichodesmium Blooms Southwest of Madagascar

Global observations of MCI with MERIS show extensive linear slicks in the southern waters of the Mozambique Channel. These tend to occur in January and February (Fig. 2.14). Spectral properties of the MERIS data suggest that these slicks are most probably due to *Trichodesmium*, though there have been reports of pelagic *Sargassum* in the area. We have no in-situ reports of these events for confirmation. The observed time series has a maximum value in January 2009. In this year, signal was also present in December and February, amounting to 18 and 15 % respectively of the January peak. In 2006, a smaller peak was observed, also in January, and in 2007, 2010 and 2012 smaller peaks were observed in February. The plot shows some presence of slicks in the southern summer of all years.

Figure 2.15 shows an image with spectra from the pattern of slicks off the south-west coast of Madagascar, on 25 January 2009, covering a significant area. The time series plot suggests the event must have lasted several weeks, with peak extent in January, but significant signal in December and February. The difference spectrum shown is similar to those for *Trichodesmium* presented above. The MCI is responding to the presence of surface slicks in its detection of *Trichodesmium* and does not detect less intense events for which such slicks do not form.

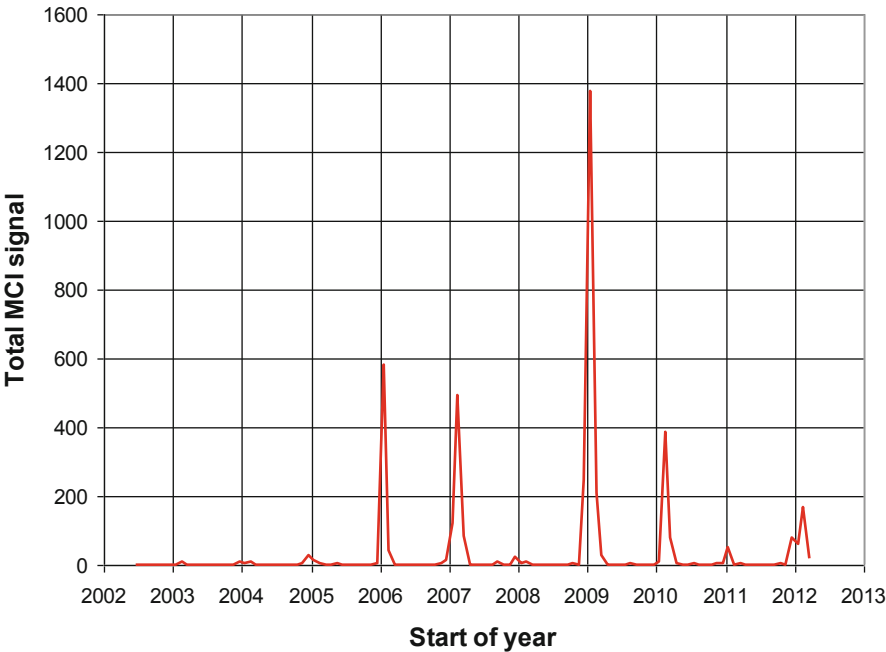


Fig. 2.14 The time series of total signal in the area 24–31°S, 36–43°E, for the waters of the Mozambique Channel, southwest of Madagascar

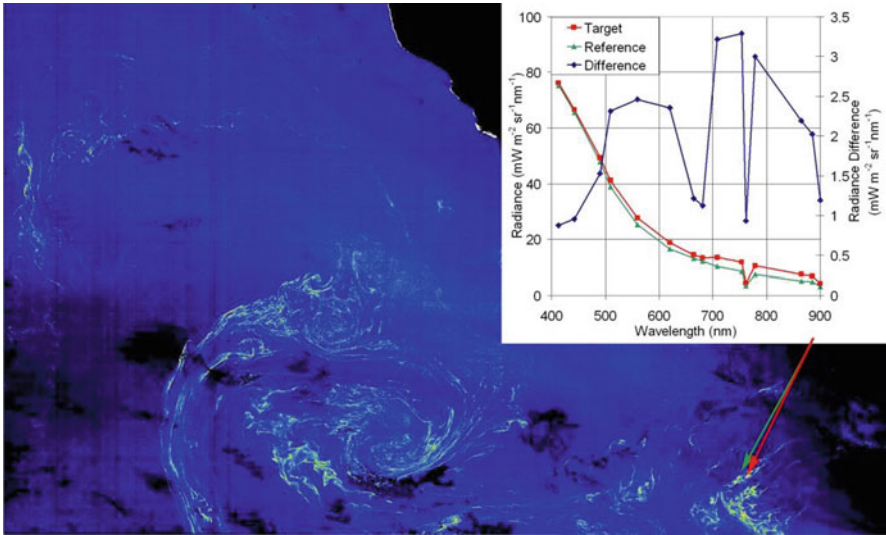


Fig. 2.15 MCI image (with spectra) of the slick pattern off Madagascar, 25 January 2009. The imaged area is about 500 km across, centred at about 26°S, 43°E. Cloud and land (*upper right*) and sun glint (*lower right*) are masked to black. Marine vegetation along the coast gives high MCI signal at upper right. The bloom spectrum is shown at top right in the same format as Figs. 2.8 and 2.9

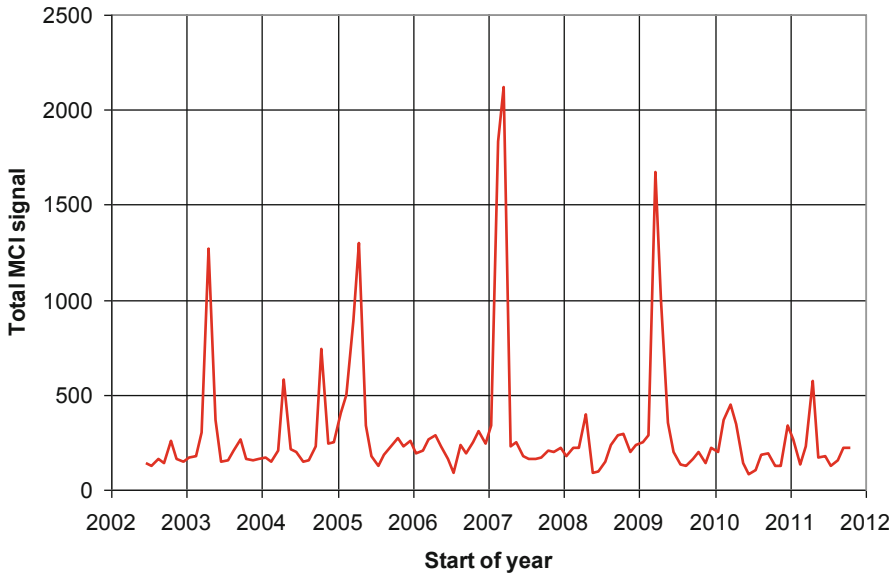


Fig. 2.16 The time series of total signal in the area 32–35°S, 15–20°E covering the waters off Cape Town, South Africa

2.9 Coastal Blooms Off South Africa

We present the statistics of blooms in two coastal areas of South Africa, one off Cape Town, and the other further east, between Cape Agulhas and Port Elizabeth. Figure 2.16 shows the time series of total signal in the Cape Town area, 32–35°S, 15–20°E, derived from the global monthly composite MCI images. This area includes coastal water and land. Because of this, the time series includes a variable background signal in all months from coastal vegetation, including coral reefs, if present. This signal is absent in Figs. 2.10 and 2.14 for the Red Sea and Mozambique Channel, which cover only open water.

Most of the peaks in Fig. 2.16 occur in April (large peaks in 2003, 2005 and March and April of 2009, and lesser peaks in April 2004, 2008 and 2011 and from February to April 2010). These are due to blooms close to shore in St Helena Bay, north of Cape Town. The largest peak shown, in February and March of 2007, is due to blooms close to the coast south of Cape Town and extending offshore to about 50 km off Cape Columbine, northwest of the city (Fig. 2.17). The only bloom outside the February to April period occurred in October 2004, mostly up to 50 km offshore of Cape Town, with some signal near shore in St Helena Bay.

The peaks in the time series in Fig. 2.16 are relatively broad, suggesting duration of bloom events of several weeks, so that signal appears in peak months and in months before and after. Figure 2.19 shows the time series for blooms in the area

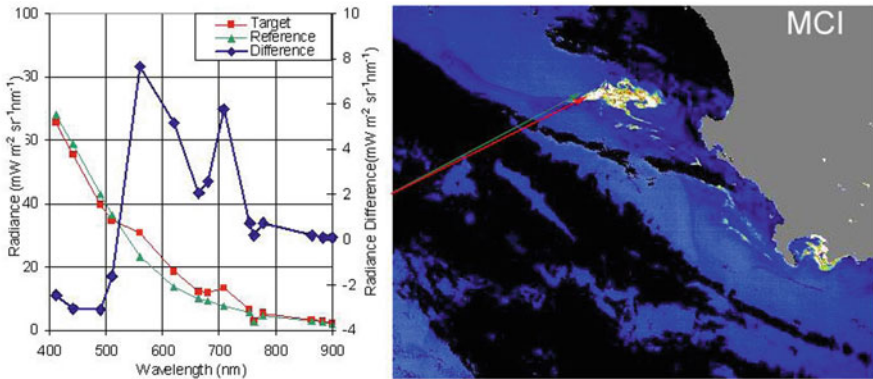


Fig. 2.17 MERIS image of high MCI signal from blooms near Cape Town, off Cape Columbine and in False Bay on 25 February 2007. The spectrum of the bloom off Cape Columbine is shown at left in the same format as Figs. 2.8 and 2.9

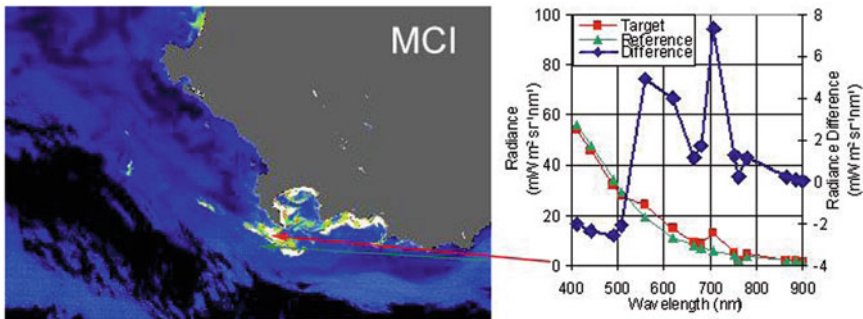


Fig. 2.18 MERIS image of the blooms on 13 March 2007 in the waters of False Bay, south east of Cape Town, South Africa. The spectrum of the bloom off False Bay is shown at right in the same format as Figs. 2.8 and 2.9

between Cape Agulhas, east of Cape Town, and East London. Here the time peaks are narrower, representing a high value in one month only, and suggesting events lasting for shorter periods. Of the three major peaks, two occur in April and one in November.

The high MCI signal indicates very high surface chlorophyll concentrations, probably at several hundreds of mg m^{-3} , due to intense blooms in surface waters on the South African coast. All events shown in Figs. 2.17, 2.18 and 2.20 show the peak at 709 nm as a major feature of the bloom spectra, with little or no added radiance at wavelengths longer than 720 nm. This indicates blooms in the near-surface waters, with no buoyant slicks covering parts of the water surface. This is in contrast to the spectra in Figs. 2.8, 2.9, 2.13 and 2.15, which show radiance increased also at longer wavelengths. This increase at longer wavelengths shows that all or most of the high-chlorophyll signal is from buoyant surface slicks of the type characteristic of *Trichodesmium*, or from floating *Sargassum*.

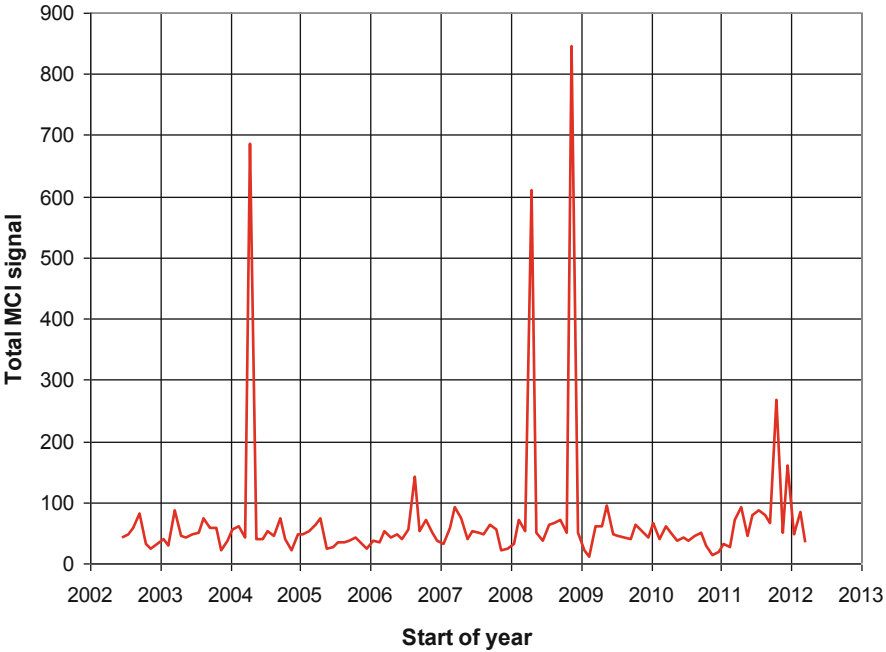


Fig. 2.19 The time series of total signal along the south coast of South Africa from east of Cape Town to East London, over the area 33–37°S, 20–28°E

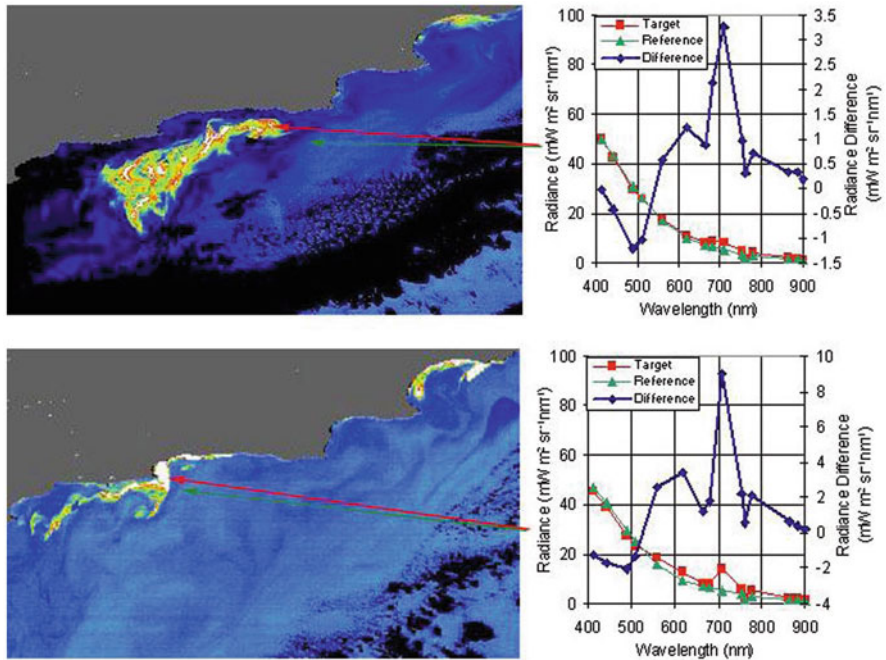


Fig. 2.20 MERIS MCI images of blooms in the waters west of Port Elizabeth, South Africa, top on 12 April 2004, bottom on 14 April 2008. In both cases, spectra show high peaks at 709 nm

We discuss above our reasons for believing that spectra shown in this chapter are from *Trichodesmium*. Pelagic *Sargassum* does not appear to be common in African waters. We have evidence for an occurrence in Sierra Leone following the equatorial Atlantic *Sargassum* event in the summer of 2011, but this appears to be unusual.

2.10 Summary and Conclusions

Ocean colour data from satellites now provide a valuable source of information on spatial and temporal patterns for all oceans and coastal waters of the world. Studies of African waters can be expected to especially benefit from satellite data, because of the lack of local observing facilities and supporting infra-structure, and the danger of piracy in some areas.

We hope that satellite water colour coverage will continue, though the recent loss of MERIS reminds us of the risk of a data gap in time. At present, images cover space scales from kilometers to global, and time scales from daily to the 15-year period for which data have been provided since 1997 by SeaWiFS, MODIS, MERIS and VIIRS. Other options, not considered here, include information on longer term trends that can be deduced by comparison of recent data with results from the CZCS (1978–1986), and the use of finer scale data from higher resolution, but less sensitive, imagers such as Landsat MSS or TM. Spatial resolution can be extended down to a scale of meters using commercial mapping sensors.

The fluorescence data from MODIS and MERIS are useful to confirm the chlorophyll values available through the green to blue ratio method. Examples are given in Figs. 2.2, 2.4, 2.5 and 2.6 above. Here we find that normalization of FLH as conventionally carried out, is not appropriate, in that un-normalized FLH provides a good measure of chlorophyll.

MERIS, through the spectral band at 709 nm, provided the added capability of detecting blooms using the MCI index. We would like to continue time series such as Figs. 2.10, 2.11, 2.12, 2.14, 2.16 and 2.19 indefinitely into the future, but there is now a data gap until the launch of ESA's Sentinel 3 satellite, planned for 2014.

Acknowledgments This work was supported by the Canadian federal Department of Fisheries and Oceans, and by the Canadian Space Agency. MODIS satellite data are made available by NASA, the US National Aeronautics and Space Administration. MERIS image data are made available by the European Space Agency, ESA. Time series analysis of MERIS data is made possible by the G-POD system of ESA. Some analyses and visualizations used in this study were produced with the Giovanni online data system, developed and maintained by the NASA GES DISC.

References

- Abbott MR, Letelier RM (1999) Algorithm theoretical basis document chlorophyll fluorescence, MODIS product number 20, NASA. http://modis.gsfc.nasa.gov/data/atbd/atbd_mod22.pdf. Accessed 27 Dec 2013
- Acker JG, Leptoukh G (2007) Online analysis enhances use of NASA earth science data. *Eos Trans AGU* 88(2):14–17

- Behrenfeld MJ, Westberry TK, Boss ES, O'Malley RT, Siegel DA, Wiggert JD, Franz BA, McClain CR, Feldman GC, Doney SC, Moore JK, Dall'Olmo G, Milligan AJ, Lima I, Mahowald N (2009) Satellite-detected fluorescence reveals global physiology of ocean phytoplankton. *Biogeosciences* 6:779–794
- Gitelson A (1992) The peak near 700 nm on radiance spectra of algae and water: relationships of its magnitude and position with chlorophyll concentration. *Int J Remote Sens* 13:3367–3373
- Gower JFR, Borstad GA (1990) Mapping of phytoplankton by solar-stimulated fluorescence using an imaging spectrometer. *Int J Remote Sens* 11:313–320
- Gower JFR, Doerffer R, Borstad GA (1999) Interpretation of the 685 nm peak in water-leaving radiance spectra in terms of fluorescence, absorption and scattering, and its observation by MERIS. *Int J Remote Sens* 9:1771–1786
- Gower JFR, Brown L, Borstad G (2004) Observation of chlorophyll fluorescence in west coast waters of Canada using the MODIS satellite sensor. *Can J Remote Sens* 30:17–25
- Gower JFR, King S, Borstad G, Brown L (2005) Detection of intense plankton blooms using the 709 nm band of the MERIS imaging spectrometer. *Int J Remote Sens* 26:2005–2012
- Gower JFR, Hu C, Borstad G, King S (2006) Ocean color satellites show extensive lines of floating *Sargassum* in the Gulf of Mexico. *IEEE Trans Geosci Remote Sens* 44:3619–3625
- Gower JFR, King S (2007a) Validation of chlorophyll fluorescence derived from MERIS on the west coast of Canada. *Int J Remote Sens* 28:625–635
- Gower JFR, King S (2007b) An Antarctic ice-related “superbloom” observed with the MERIS satellite imager. *Geophys Res Lett* 34. doi:10.1029/2007GL029638
- Gower JFR, King S, Borstad G, Brown L (2008a) The importance of a band at 709 nm for interpreting water-leaving spectral radiance. *Can J Remote Sens* 34:287–295
- Gower JFR, King SA, Goncalves P (2008b) Global monitoring of plankton blooms using MERIS MCI. *Int J Remote Sens* 29:6209–6216
- Gower JFR, King S (2011) Distribution of floating *Sargassum* in the Gulf of Mexico and Atlantic Ocean mapped using MERIS. *Int J Remote Sens* 32:1917–1929
- Morel A, Prieur L (1977) Analysis of variations in ocean color. *Limnol Oceanogr* 22:709–723
- Moulin C, Gordon HR, Chomko RM, Banzon VF, Evans RH (2001) Atmospheric correction of ocean color imagery through thick layers of Saharan dust. *Geophys Res Lett* 28:5–8
- Singh RP, Prasad AK, Kayetha VK, Kafatos M (2008) Enhancement of oceanic parameters associated with dust storms using satellite data. *J Geophys Res* 113(C11008). doi:10.1019/2008JC004815
- Yacobi YZ, Gitelson A, Mayo M (1995) Remote sensing of chlorophyll in Lake Kinneret using high spectra resolution radiometer and Landsat TM: spectral features of reflectance and algorithm development. *J Plankton Res* 17:2155–2173

<http://www.springer.com/978-94-017-8007-0>

Remote Sensing of the African Seas

Barale, V.; Gade, M. (Eds.)

2014, XXIX, 428 p. 187 illus., 124 illus. in color.,

Hardcover

ISBN: 978-94-017-8007-0